frontiers in Earth Science

ORIGINAL RESEARCH
published: 08 May 2019
doi: 10.3389/feart.2019.00098

Chemical and Isotopic Evidence for Organic Matter Sulfurization in Redox Gradients Around Mangrove Roots

M. R. Raven[1], D. A. Fike[2], M. L. Gomes[3] and S. M. Webb[4]*

[1] Department of Earth Sciences, University of California, Santa Barbara, Santa Barbara, CA, United States, [2] Department of Earth and Planetary Sciences, Washington University in St. Louis, St. Louis, MO, United States, [3] Department of Earth and Planetary Sciences, Johns Hopkins University, Baltimore, MD, United States, [4] Stanford Synchrotron Radiation Lightsource, Stanford University, Menlo Park, CA, United States

Coastal environments like mangrove forests are increasingly recognized as potential hotspots for organic carbon burial, giving them a crucial and yet poorly constrained role in the global carbon cycle. Mangrove sediments are frequently anoxic, which facilitates elevated organic matter (OM) burial via several mechanisms, including sulfurization – abiotic reactions between dissolved (poly)sulfide and OM that decrease its lability. Although sulfurization was estimated to account for roughly half of OM preservation in a Bermuda mangrove forest, both its mechanisms and its global significance remain poorly understood. In this study, we investigate S cycling in mangrove forest sediments from Little Ambergris Cay, Turks and Caicos Islands, an environment with predominantly microbial OM inputs and no major source of terrestrial iron. We characterize the S- and C-isotope composition and organic S speciation of sedimentary OM fractions with varying degrees of resistance to acid hydrolysis, along with other inorganic S phases. Near the surface of a 3-mm-diameter, O_2-releasing root, abundant organic and elemental S with a ^{34}S-depleted composition indicates microbial sulfur cycling and OM sulfurization. A mixture of pyrite, elemental S, and organic S form a plaque within the outer 50 μm of the root, which also contains strongly ^{34}S-depleted sulfate in its xylem. OM sulfurization products in the sediments include both the alkyl sulfides and disulfides associated with the root plaque and more oxidized forms, especially sulfonates. Hydrolysis-resistant organic S in the sediments is consistently 3–5‰ more ^{34}S-enriched than coexisting elemental S, matching the reported kinetic isotope fractionation factor for OM sulfurization via reaction with polysulfides. These sediments also contain a substantial pool of solid-phase, hydrolyzable organic S with a seawater sulfate-like isotope composition, largely in the form of sulfate esters, which may represent excretions from abundant gastropods. The coexistance of sulfurized OM and aerobic macrofauna highlights how understanding spatial scales and/or temporal cycles in local redox state is critical for predicting net OM preservation, especially in

OPEN ACCESS

Edited by:
Samuel Abiven,
University of Zurich, Switzerland

Reviewed by:
Gonzalo V. Gomez-Saez,
University of Oldenburg, Germany
Alexey Kamyshny,
Ben-Gurion University of the Negev, Israel

****Correspondence:***
M. R. Raven
raven@ucsb.edu

Specialty section:
This article was submitted to Biogeoscience, a section of the journal Frontiers in Earth Science

Received: *21 November 2018*
Accepted: *18 April 2019*
Published: *08 May 2019*

Citation:
Raven MR, Fike DA, Gomes ML and Webb SM (2019) Chemical and Isotopic Evidence for Organic Matter Sulfurization in Redox Gradients Around Mangrove Roots. Front. Earth Sci. 7:98. doi: 10.3389/feart.2019.00098

dynamic, coastal environments. Future attempts to mechanistically predict changes in carbon storage in coastal systems will benefit from incorporating OM sulfurization as both a sink for microbially produced sulfide and a mechanism for enhanced carbon sequestration.

Keywords: X-ray absorption spectoscropy, sulfur isotope, coastal carbon cycle, organic sulfur, organic matter lability, mangrove sediment, sulfurization

INTRODUCTION

Mangrove sediments are important loci of organic matter (OM) preservation and burial, accounting for 10–15% of coastal carbon preservation on Earth today (Alongi, 2014) or an average burial flux of 24 Tg C/yr globally (Twilley et al., 1992; Jennerjahn and Ittekkot, 2004; Duarte and Prairie, 2005; Kristensen et al., 2008). At the same time, mangrove ecosystems are susceptible to disruption associated with changes in land use, restoration activities, habitat migration, and sea level on both human and geologic timescales (Gilman et al., 2008; Ellison and Zouh, 2012; Lovelock et al., 2015). Despite the potential importance of these critical environments for the global C cycle, there is a great deal we do not yet understand about the mechanisms controlling OM preservation in mangrove forest sediments.

Elevated organic C burial fluxes in mangrove sediments result from both elevated OM inputs and limited OM degradation. Mangrove litterfall (leaves) generally represents ∼25% or less of the net primary productivity of a mangrove forest, with other organic C inputs including belowground mangrove biomass (wood and roots), planktonic, benthic, and epiphytic phototrophs, and terrestrial detritus (Jennerjahn and Ittekkot, 2004; Kristensen et al., 2008). This abundant OM fuels high organic C remineralization rates in shallow mangrove sediments (on the order of 20–200 mmol/m^2/d; Kristensen et al., 2008), which cause rapid consumption of dissolved oxygen in pore water. Once conditions are anoxic, multiple processes suppress rates of carbon remineralization. Less metabolic energy for growth is available for microorganisms that reduce sulfate or other electron acceptors in place of O_2, and many exoenzymes that break down macromolecular OM for consumption operate only under oxic conditions (Kristensen et al., 1995; Hulthe et al., 1998; Burdige, 2007). Further, bioturbating macrofauna like crustaceans and mollusks that consume sedimentary OM (Middelburg and Levin, 2009; Jessen et al., 2017) have only a limited tolerance for anoxic conditions (Aguirre-Velarde et al., 2018). Dissolved sulfide generated from microbial sulfate reduction can accumulate in pore water (Jorgensen, 1982), which further limits the distribution of many metazoans. Importantly, dissolved sulfide can also react abiotically to "sulfurize" OM and reduce its lability (Brassell et al., 1986; Boussafir et al., 1995). Understanding the impacts of these processes on sedimentary OM cycling is critical for evaluating how rates of organic C burial may vary under future scenarios of environmental change.

Sulfurization is frequently a major contributor to OM preservation in OM-rich, anoxic, open marine sediments, in both modern and ancient systems (Francois, 1987; Eglinton et al., 1994; Wakeham et al., 1995; Raven et al., 2019). Recent work has found that sulfurization occurs more rapidly, and in a broader range of environments, than previously realized, including hydrothermal systems (Gomez-Saez et al., 2016), sinking marine particles (Raven et al., 2016, 2019), and surface sediments exposed to variable redox conditions (Jessen et al., 2017). However, relatively little is known about how this process impacts the preservation of carbon in coastal ecosystems. OM sulfurization in mangrove sediments was first observed in a Thai mangrove forest (Holmer et al., 1994) and further explored in a study of Mangrove Bay, Bermuda (Canfield et al., 1998). Measured rates of microbial sulfate reduction in Mangrove Bay are extremely high – up to 25 μM/hr (Boudreau et al., 1992) – and it was estimated that sulfurization contributed roughly half of the buried organic S in that system, with the remainder having a seawater sulfate-like S-isotope composition (Canfield et al., 1998).

Sulfurization increases the preservation potential of OM by replacing energy-rich moieties like alcohols, aldehydes, and conjugated double bonds and generating high-molecular-weight polymers that are thought to be less amenable to breakdown and utilization by microorganisms (Kohnen et al., 1989; Boussafir et al., 1995; Hebting et al., 2006). Experimental data indicate that the key reactants for sulfurization on short timescales (hours to weeks) are polysulfides (S_x^{2-}, where x = 2–7), which are highly reactive, rapidly equilibrating dissolved species (Kohnen et al., 1991; Amrani and Aizenshtat, 2004; Raven et al., 2016) that form spontaneously from dissolved sulfide in the presence of elemental sulfur or other mild oxidants (Rickard and Luther, 2007). Accordingly, although they are challenging to measure directly in the field, polysulfides can be thermodynamically favorable and potentially quite abundant near redox interfaces in water columns, sediments, hydrothermal systems, or microbial mats (Luther et al., 2001; Rickard and Luther, 2007; Findlay, 2016; Findlay and Kamyshny, 2017). In mangrove sediments, redox gradients are generated by O_2-releasing roots of species like *Rhizophora mangle, Avicennia germinans*, and *Laguncularia racemosa*, burrowing macrofauna, and, in some cases, the surface layers of benthic microbial mats. These redox gradients are favorable locations for polysulfide formation and are thus potential hotspots for S_x^{2-}–driven OM sulfurization.

Here, we present results for the abundance, isotopic composition, and speciation of solid-phase S in mangrove sediments, including multiple pools of organic S. Our samples come from Little Ambergris Cay, Turks and Caicos Islands, where low iron availability, the absence of significant terrestrial detritus, and thick microbial mats allow us to isolate the effects of biogeochemical sulfur cycling on OM sulfurization reactions in an end-member-type mangrove forest environment. By investigating patterns in the distribution and chemical form

of S in these sediments, we can assess the significance of OM sulfurization for preserving and burying microbial carbon in mangrove ecosystems and the role of aerating mangrove roots in this process.

Study Site

Little Ambergris Cay is an uninhabited island in the southern portion of the Turks and Caicos Islands, British West Indies, located in the Atlantic, south of the Bahamas (**Figure 1**). Siliciclastic influx is insignificant in this marine carbonate platform (Wanless and Dravis, 2008). The emergent island is composed of a bedrock rim of ooid grainstone surrounding a shallow bay lined with mangroves and microbial mats (Orzechowski et al., 2016; Stein et al., 2016). Tidal pumping and storms are removal mechanisms for mangrove leaf litter. Besides the mangrove wood and roots, organic carbon production in these systems is mostly from benthos, similar to observations from mangrove environments in Florida and Belize (Wooller et al., 2003). Microbial mats with various morphologies are common in the island's inner channels and bays (Gomes et al., 2016; Stein et al., 2016; Trembath-Reichert et al., 2016). Production in these mats is mostly cyanobacterial, and O_2 penetration is typically very shallow (∼1–5 mm during the day; Trembath-Reichert et al., 2016). Accordingly, Little Ambergris Cay represents an end-member case, with OM influxes dominated by benthic microbial mats and/or below-ground mangrove production rather than mixed terrestrial, litterfall, or algal sources. It contrasts mangrove systems dominated by fluvial sediment input and peat generation like the Maira-gawa mangrove area on Iriomote Island, Japan (Mazda and Ikeda, 2006).

MATERIALS AND METHODS

We investigated OM and S pools in two samples of mangrove sediments containing allochthonous concentrically laminated carbonate grains (ooids) from Little Ambergris Cay. Sediment samples were collected from the edge of the southeastern bay (N21.29298°, W71.70636°) in August 2017 (**Figure 1**), stored in sealed bags at 2°C, and sectioned under an O_2-free atmosphere. Two samples were analyzed: (1) bb10, in which a ∼3 mm-diameter, presumably O_2-releasing portion of a mangrove root is surrounded by dark brown, spongey, ooid-rich sediments and overlain by a ∼2-cm-thick gray surface microbial mat; and (2) bb07, which contains ∼2-cm-diameter woody trunk that is surrounded by less apparent organic-rich material and no visible microbial mat. Images of subsamples are shown in **Figure 2**. For bb10, a thin layer of lighter-colored material along an exposed field sampling surface was isolated as sample "S." Sediments in the 1–2 cm zone surrounding the ∼3 mm-diameter mangrove root ("R") were split in half as shown in **Figure 2D**. Spongey brown sediments containing micro-roots were divided into two

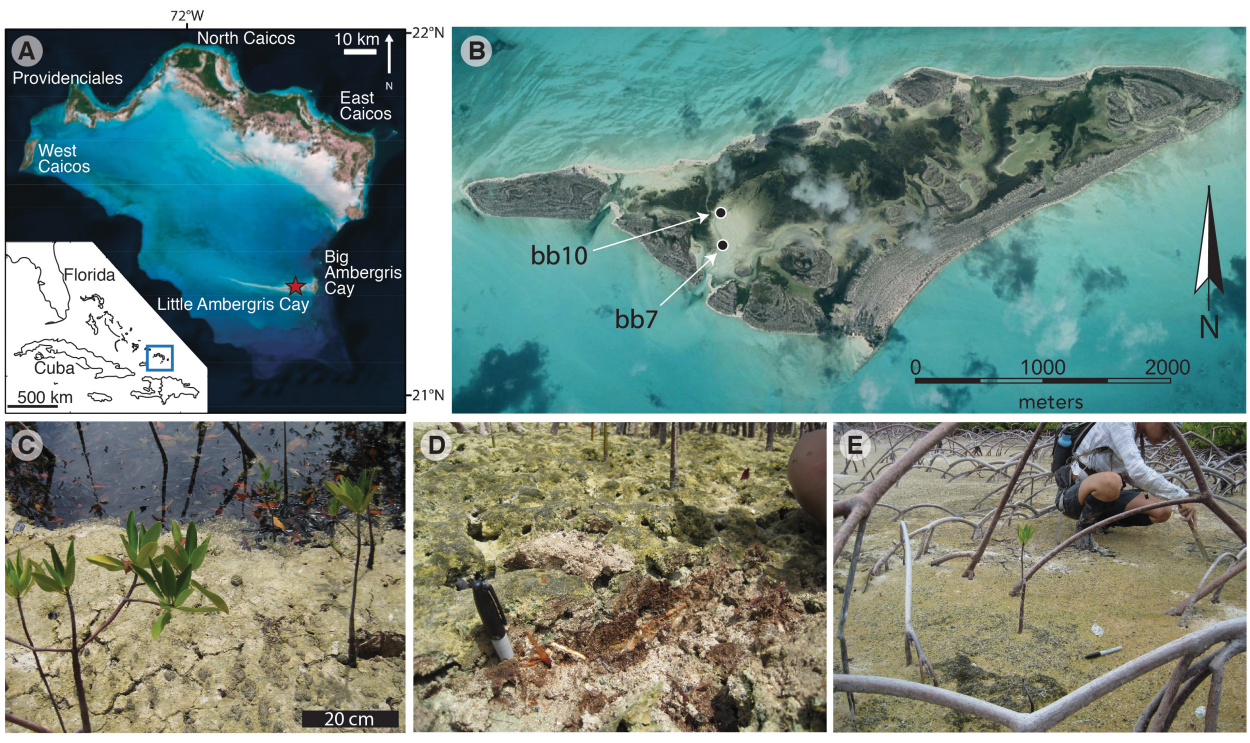

FIGURE 1 | Geographic setting and site photos. **(A)** Location of the Turks and Caicos Islands within the southwest North Atlantic Ocean and Little Ambergris Cay within the Caicos platform (Trembath-Reichert et al., 2016); **(B)** Image of Little Ambergris Cay (image from Google Earth with map data from SIO, NOAA, U.S. Navy, NGA, GEBCO; image 2019 DigitalGlobe); **(C)** Site bb10; **(D)** Exposure of peat-textured material near bb10; **(E)** Site bb07.

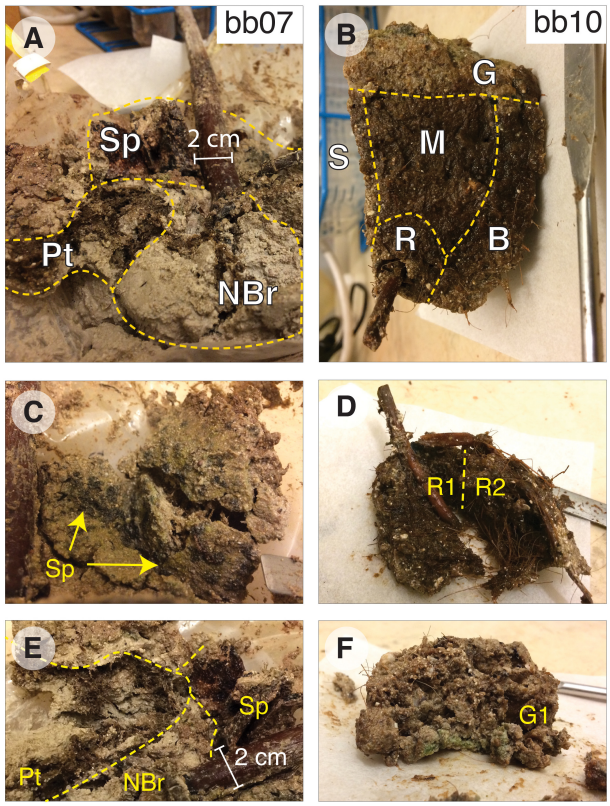

FIGURE 2 | Images of sediment samples. Samples were subdivided in an anaerobic chamber based on differences in sediment texture, color, and structure. Sample bb07 **(A,C,E)** included three distinctive textures: sands adjacent to the juvenile trunk ("NBr" and "NP"), cohesive sheets with black spots ("Sp," **C**), and spongey brown materials ("Pt," **E**). Sample bb10 **(B,D,F)** was divided into a side layer that was most susceptible to exposure during initial sampling ("S"), a region within ~1 cm of a root with few gastropods ("R," **D**), gastropod-rich or -poor brown spongey materials ('M' and 'B,' respectively), and a gray sandy surface mat ("G," **F**). Multiple subsamples for each region were not homogenized and instead represent spatially coherent sub-divisions of the region **(D)**. The spatula for scale in panels **B**–**D** and **F** measures 0.8 cm across its flat end.

sections with abundant gastropods (21–27 wt%, M1 and M2) and one section with less abundant gastropods (8 wt%, B). The surface microbial mat was separated by color into green-gray (G1, see **Figure 2F**) and warm brown portions (G2, G3). For sample bb7, near-trunk, carbonate-rich materials were separated based on their brownish or pinkish coloring (NBr and NP, respectively). Certain spatially coherent zones were composed of brown materials with a peaty texture (Pt, see **Figure 2E**). We also observed a cohesive sandy layer with distinctive black spots, surrounding the juvenile trunk at a distance of a few centimeters (Sp, **Figure 2**).

We used a sequential extraction procedure to separate operationally defined pools of organic and inorganic S. Samples were washed with O_2-free water to remove salts and then microwave-extracted with 9:1 dichloromethane:methanol. Organic extracts were separated on silica gel with 4:1 hexane:dichloromethane to elute non-polar compounds, including elemental S. One split of this non-polar fraction was exposed to activated copper pellets (10 h, room temperature, with occasional agitation) to remove S^0 and quantify S in non-polar organic extracts; reported S^0 concentrations and $\delta^{34}S$ values are corrected for S in non-polar lipids. The remaining extracted solids were divided in half. One split was used for a stepped hydrolysis experiment, with aliquots collected after each of two steps: mild hydrolysis (1N HCl, 1 h, 20°C) to dissolve calcium carbonate, and moderate hydrolysis (6N HCl, 2 h, 70°C) to solubilize the operationally defined low-temperature hydrolyzable OS pool. The second split of the extracted solids was acidified in a gas-tight distillation apparatus under more intense hydrolysis (6N HCl, 4 h, 176°C) to trap acid-volatile S (AVS), and then Cr^{+2} solution (~3M $CrCl_2$ in 6N HCl, 4 h, 176°C) to distill chromium-reducible S (CRS) and trap it in 1M Zn acetate solution as ZnS (Canfield et al., 1986; Burton et al., 2008); residual solids were washed in DI water and freeze-dried. All temperatures listed here represent equipment setpoints and are practically ±5°C. Solid-phase samples were analyzed at Washington University in St. Louis to measure their S and C concentrations, $\delta^{13}C$ values, and $\delta^{34}S$ values. Extracted inorganic S phases (S^0, AVS, and CRS) were quantified after oxidation to sulfate (30% H_2O_2, 70°, 24 h) by ion chromatography (Metrohm 881 ion chromatograph on a Metrosep A Supp7 150 mm × 4.0 mm anion column), precipitated as $BaSO_4$ (with excess $BaCl_2$ in ultra-pure water), and analyzed for $\delta^{34}S$ by combustion EA-IRMS (Costech 4010 EA + Thermo Delta V Plus, configured for S). C-isotope analyzes and TOC concentrations were also made by combustion EA-IRMS (Thermo Flash 2000 EA with zero-blank autosampler + Delta V Plus, configured for C). Reported $\delta^{34}S$ and $\delta^{13}C$ values have estimated analytical uncertainties (1 SD) of ±0.2‰ and ±0.1‰, respectively, based on long-term standard reproducibility.

Using this sequential extraction procedure, we were able to quantify the concentration and $\delta^{34}S$ values of five pools of organic and inorganic S (**Supplementary Table 1**): (1) zero-valent sulfur (S^0), (2) moderate-temperature hydrolyzable OS_{Hy}, (3) high-temperature hydrolyzable OS_{Hy}, (4) chromium reducible sulfides (CRS: mostly pyrite; Canfield et al., 1986), and (5) non-hydrolyzable S (OS_{Res}). Minimal recovery of AVS (<1.1 μmol/g, **Supplementary Table 1**) precluded S-isotope analysis of that pool. Reported S^0 concentrations and $\delta^{34}S$ values are corrected for S in non-polar lipids by comparing the split exposed to activated copper pellets to the split not treated with activated copper; polar lipids were not analyzed further for this study. The abundance and S-isotope composition of moderate-temperature OS_{Hy} were calculated as the difference between the solids remaining after moderate (70°C) and mild (20°C) hydrolysis. The abundance and S-isotope composition of high-temperature OS_{Hy} were calculated as the difference between the solids remaining after CRS extraction (176°C) and moderate (70°C) hydrolysis, accounting for CRS removal during the high temperature treatment. Together, the moderate and high temperature pools constitute total hydrolyzable OS (OS_{Hy}). Remaining solid-phase S after CRS extraction constitutes "residual" OS (OS_{Res}) and is equivalent to the "NonCROS" pool in Canfield et al. (1998). Concentrations of carbon

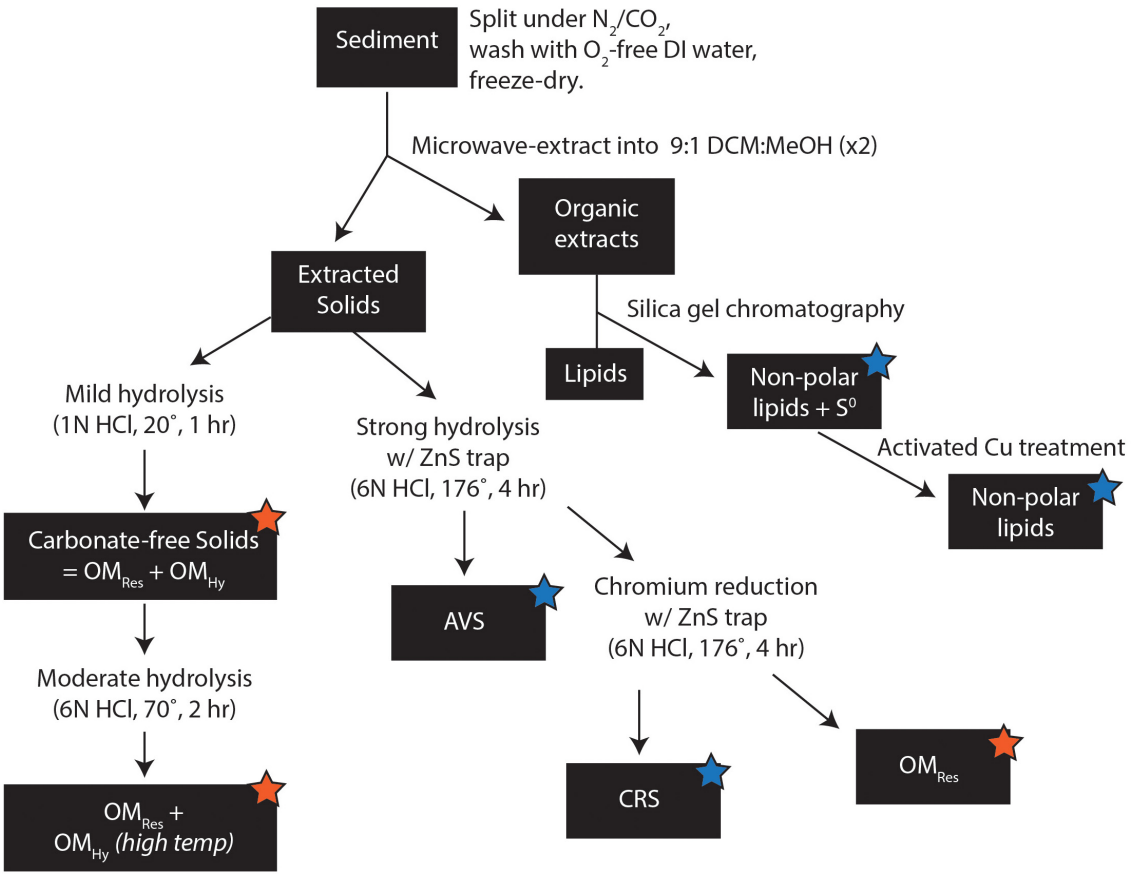

FIGURE 3 | Sample preparation methods. Orange stars indicate fractions analyzed for S content and $\delta^{34}S$ by EA-IRMS and S-speciation by XAS; blue stars indicate fractions analyzed only for S content and $\delta^{34}S$ by EA-IRMS.

and $\delta^{13}C$ values of the organic pools (moderate-temperature OS_{Hy}, high-temperature OS_{Hy}, and OS_{Res}) were also quantified using this scheme.

In order to determine the bonding environment of organic S, three aliquots of each sample (following mild, moderate, and strong hydrolysis, see stars in **Figure 3**) were analyzed by X-ray absorption spectroscopy at the Stanford Synchrotron Radiation Lightsource (SSRL) at the SLAC National Accelerator Laboratory. Sulfur K-edge spectra were collected on beam line 14–3, a bending magnet workstation with a flux of 2×10^{10} photons/sec. The incident X-ray beam was set to a size of 500 μm × 1000 μm and the energy calibrated to the sodium thiosulfate ($Na_2S_2O_3$) pre-edge peak at 2472.02 eV. Spectra were processed using SIXPACK (Webb, 2005), using linear pre- and post-edge normalization for background removal. Similar methods, but with a smaller 10 μm × 10 μm beam size obtained by focusing the beam with a Kirkpatrick-Baez mirror pair, were used to map root S speciation across a 0.5 mm wide × 3 mm region of the freeze-dried, split mangrove root from sample bb10. Maps were collected for six X-ray energies associated with distinctive spectral features of various S phases (2472.5, 2473.0, 2473.8, 2476.0, 2482.3, and 2482.7 eV). Finally, root samples were freeze-dried, powdered by mortar and pestle, and analyzed for total S content and $\delta^{34}S$ by EA-IRMS as above.

RESULTS

Carbon and Sulfur Pools in Sediments

After extraction with organic solvents and carbonate removal with 1N HCl, sediment samples consist mostly of OM, with TOC concentrations ranging from ∼40 wt% (bb07_Sp2, NP) to nearly 48 wt% (bb10_R2). Roughly half of this (organic solvent–insoluble) OM_{Tot} is hydrolyzable in 6N HCl at 176°C (**Figure 4**) and the other half is resistant. Due to dilution with variable amounts of carbonate, on a whole-sediment basis, these TOC concentrations are equivalent to between 3.1 wt% (in bb07_Pt1) and 20.7 wt% TOC (in bb10_M1). Broadly, whole-sediment OM concentrations are highest in the dark brown, spongey sediment from bb10 (12.1–20.7 wt% TOC), moderate in the overlying gray mat and the exposed surface layer bb10_S (5.0–8.0 wt% TOC), and lowest in sample bb07 (3.1–4.2 wt% TOC). The OM in all of our samples contains elevated ^{13}C, with $\delta^{13}C$ values ranging from −11.7‰ (bb07_Sp1) to −15.3‰ (bb10_R1). The hydrolyzable and residual portions of OM_{Tot} (OM_{Hy} and

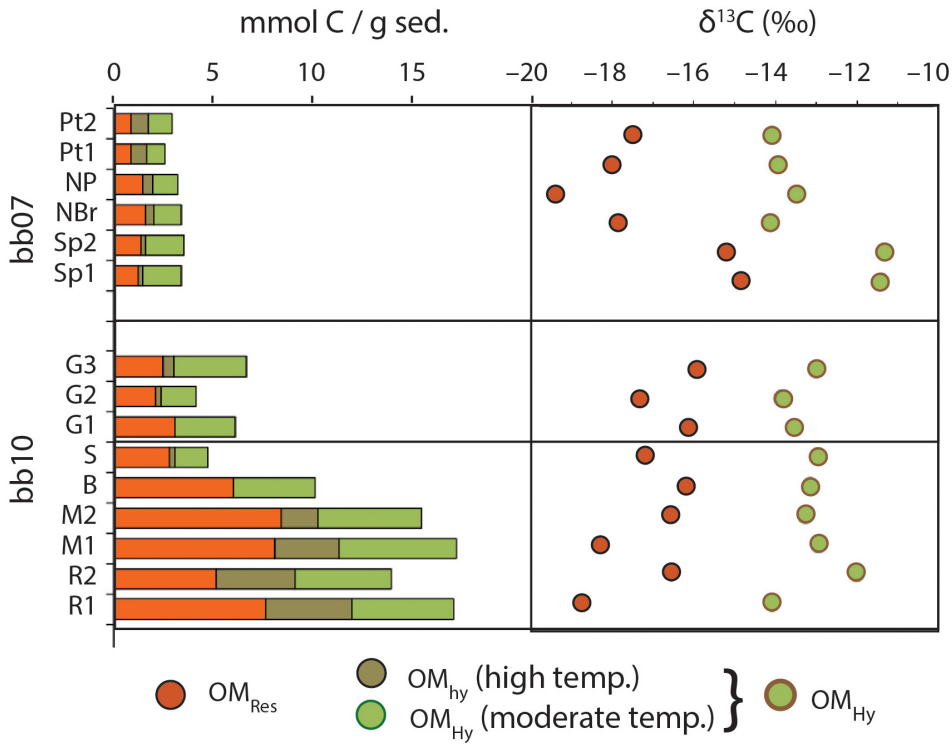

FIGURE 4 | Abundance and C-isotope composition of OM in Little Ambergris Cay sediments. Sample ordering on the *y*-axis is designed to group sub-samples of similar materials together but is otherwise arbitrary (see images in **Figure 2**). OM_{Hy} abundances are shown separately for moderate- and high-temperature hydrolysis; $\delta^{13}C$ values are shown for the total OM_{Hy} pool, calculated from summing the low-and mid-temp pools. Uncertainties on $\delta^{13}C$ values are smaller than symbols (±0.15‰, 1σ).

OM_{Res}, respectively) have significantly and consistently different C-isotope compositions, with OM_{Res} an average of 3.9‰ more ^{13}C-depleted than OM_{Hy} (**Figure 4**).

Concentrations of elemental S, CRS, OS_{Hy} and OS_{Res} are all highest in the dark, spongey portions of sample bb10 (R, M, and B, **Figure 5**). Sample bb10_R1 contains the maximum concentrations of OS_{Res} (94 μmol/g) as well as S^0 (55 μmol/g) and CRS (19 μmol/g). In contrast, in sample bb07_Sp(1,2), OS_{Res} concentrations are ∼2 μmol/g. Part of this difference in OM_{Res} concentrations stems from variable amounts of carbonate. Importantly, however, the S:C ratios of OM_{Res} in these samples also vary spatially, ranging from a maximum of 1.2 mol of S per 100 mol of C (hereafter, mol%) in bb10_R1 to a minimum of 0.2 mol% in bb07_Sp(1,2). The average S:C ratio of OM_{Hy} (3.0 mol%) is substantially higher than that of OM_{Res}, (0.7 mol%), and OM_{Hy} S:C ratios do not show any obvious spatial pattern (**Figure 5**).

The S-isotope compositions of OM_{Res} and OM_{Hy} from the same sample differ by more than 20‰. OM_{Res} is more ^{34}S-depleted, similar to concurrent S^0 and CRS where data are available. OM_{Res} is most strongly ^{34}S-depleted in the relatively S-rich parts of the bb10 sediment (R, M, and B), reaching −23‰ or a ∼45‰ offset from local sulfate (21.9 ± 0.2‰; Trower et al., 2018). In bb10_G3, both OM_{Res} and S^0 are less ^{34}S-depleted, at −11 to −15‰. OM_{Res} $\delta^{34}S$ values range from −11.3 to −1.7‰ in sample bb07, although no S^0 $\delta^{34}S$ data are available for comparison.

Sulfur Speciation by X-ray Absorption Spectroscopy (XAS)

The XAS speciation of OS is broadly consistent for multiple samples from the same region and varies systematically between regions (**Figure 6**). Hydrolyzable OS in all of the samples is predominantly (58–94%) in oxidized forms: sulfonates and especially sulfate esters. All of the OS_{Hy} samples contained moderate amounts of disulfides (6–23%) and very low amounts of sulfoxides (≤3%). The greatest source of variability among the OS_{Hy} samples is in the amount of alkyl sulfides in this pool, which represent 0–26% of OS_{Hy} (up to 38 μmol S/g). Small amounts of aromatic OS were observed in OS_{Res} but not OS_{Tot}; they may either have been unresolved in the latter spectra or they may have formed during 176°C 6N HCl treatment. Iron monosulfides (FeS) were not detected in any sediment samples, consistent with AVS results.

Unlike OS_{Hy}, OS_{Res} is dominated by reduced forms of S, especially alkyl sulfides. Sulfides become increasingly dominant in the abundant OS_{Res} pool near the bb10 root, and represent 68% of OS_{Res} or as much as 145 μmol S/g in bb10_R1. Disulfides and aromatic structures comprise relatively consistent proportions of

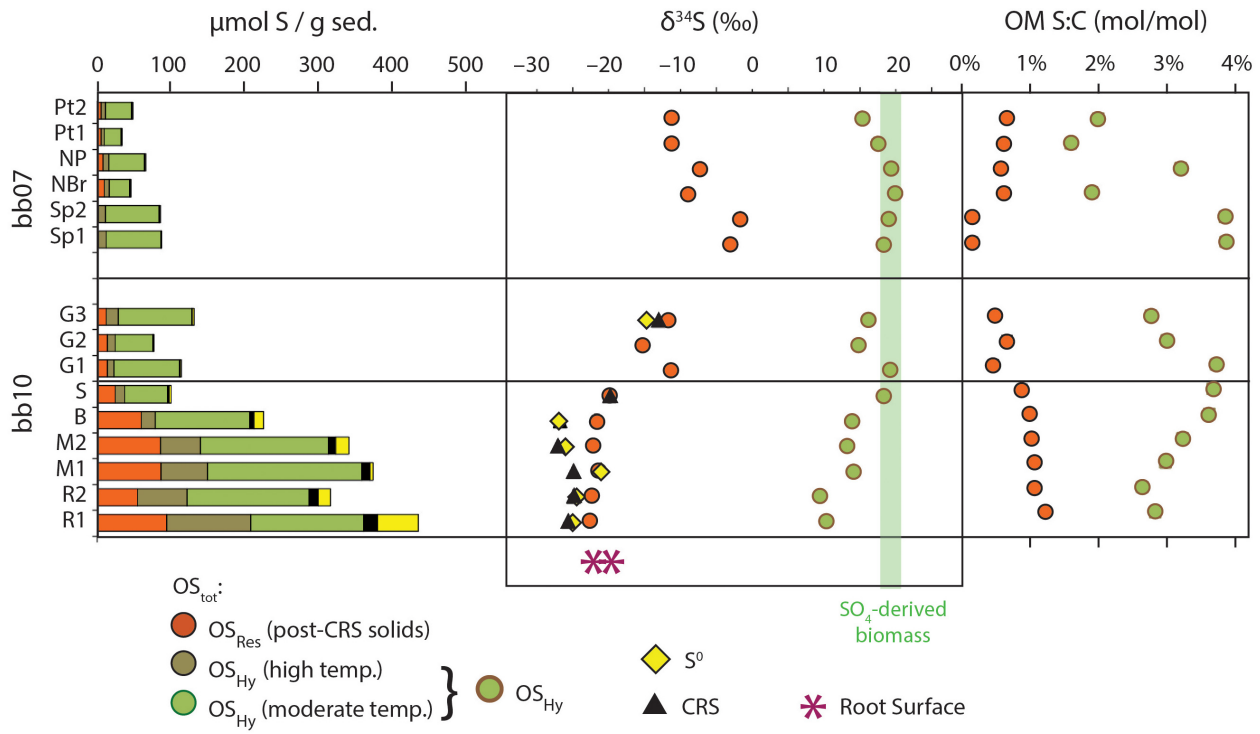

FIGURE 5 | Sulfur pools in mangrove sediments. Sample ordering on the *y*-axis is the same as in **Figures 4**, **6**. Concentrations are relative to total dry sediment mass. AVS concentrations are too low to be visible at this scale (≤1.1 µmol/g). The green shaded vertical bar represents anticipated values of biomass derived from sulfate assimilation (Kaplan and Rittenberg, 1964). The pink asterisks represent the $\delta^{34}S$ values of total S in two splits of the bb10 root cortex. Analytical uncertainties in $\delta^{34}S$ and S:C data are smaller than symbols; however, values for OS_{Hy} were calculated by difference and therefore have larger estimated (1 SD) uncertainties of ~2‰ for $\delta^{34}S$ (e.g., $\delta^{34}S = -10 \pm 2$‰) and ~7% relative for molar S:C (e.g., S:C = 1.0 ± 0.07 mol%).

OS_{Res}, averaging 16 and 15% (n = 14), respectively. Sulfonates represent a substantial proportion of OS in bb10_G samples (averaging 29% of OS_{Res} or 3.9 µmol/g) and an even larger quantity in bb10_M (15.4 µmol S/g). Sulfonates represent only ~6% of OS or 4.5 µmol S/g in bb10_R.

Two-dimensional XAS mapping (**Figure 7**) shows that sulfur is present in two distinct zones of the bb10 root: the outermost ~50 µm of the root surface, and the vascular tissues in the central root. At the root surface, S is present as a mixture of organic and inorganic phases with various redox states, including pyrite, organic sulfides and disulfides, sulfate, and S^0. Within the vascular tissues, S consists of more than 90% sulfate with smaller, poorly constrained amounts of S^0 and reduced organic S. Root tissues after removal of the outer cortex contained 0.97 wt% S with a $\delta^{34}S$ value of −7.2‰, while two sections of the outer cortex contained 2.2 and 2.7 wt% S with $\delta^{34}S$ values of −19.6 and −22.2‰, respectively.

DISCUSSION

Separation of Hydrolyzable and Residual OM

Sedimentary OM_{Tot} can be categorized based on its resistance to hydrolysis with high-temperature (176°C) hydrochloric acid, illustrated schematically in **Figure 8**. Resistance to strong acid hydrolysis is a meaningful, although imperfect, indicator of the susceptibility of OM to breakdown by extracellular hydrolytic enzymes, a key factor limiting rates of microbial heterotrophy in the environment (Chróst, 1991; Burdige, 2007; Arnosti et al., 2014). Broadly, because OM_{Hy} can be released from high-molecular-weight "proto-kerogen" by a hydrolytic mechanism, it should have a lower preservation potential than OM_{Res}. Therefore, we use OM_{Hy} and OM_{Res} to represent materials with lower or higher preservation potentials, respectively.

The $\delta^{34}S$ values of concurrent OM_{Res} and OM_{Hy} in Little Ambergris Cay sediments are dramatically different (**Figure 5** and **Table 1**), which constrains the source(s) of S to each

TABLE 1 | Summary of the characteristics of hydrolyzable and residual OM.

	OM_{Hy}	OM_{Res}
S:C ratio	1.6–3.9%	0.2–1.2%
$\delta^{34}S$	+10 to +20‰ (sulfate-like)	−1 to −23‰ (sulfide-like)
$\delta^{13}C$	Strongly ^{13}C-enriched	^{13}C-enriched, but ~4‰ less than OM_{Hy}
S species	Sulfate esters > sulfonates > (disulfides, sulfides) > sulfoxides	Sulfides > > (sulfonates, disulfides) > (esters, sulfoxides)

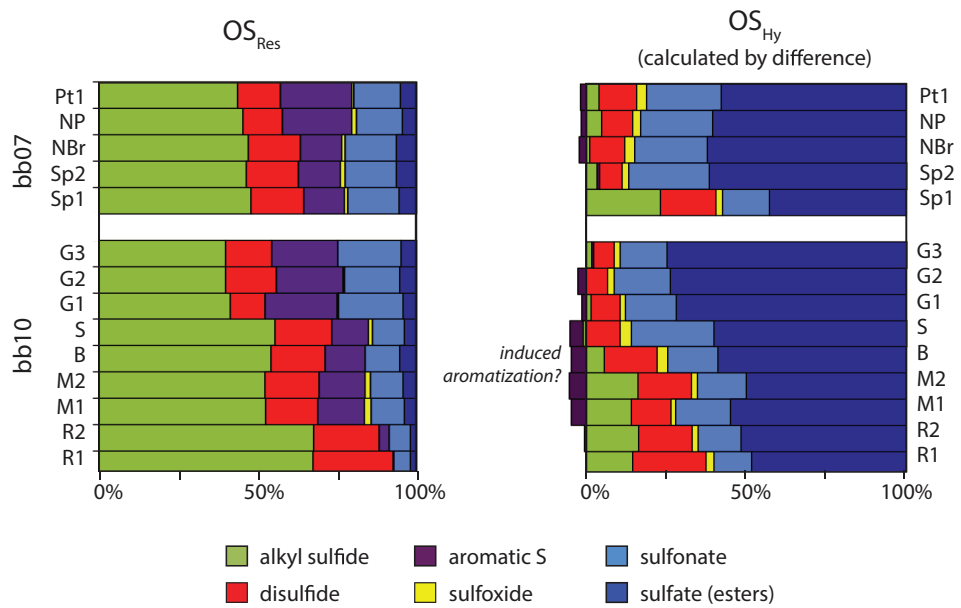

FIGURE 6 | Redox speciation of OS_{Res} and OS_{Hy}. Relative abundance of organic S with different redox states within the OS_{Res} pool, with the same vertical ordering as **Figures 4**, **5**. OM_{Hy} speciation was calculated as the difference in absolute amounts of each S moiety between sediments after mild and strong hydrolysis. Small amounts of aromatic S moieties were calculated as having negative "losses," shown as negative relative abundances, potentially suggesting their formation during strong hydrolysis.

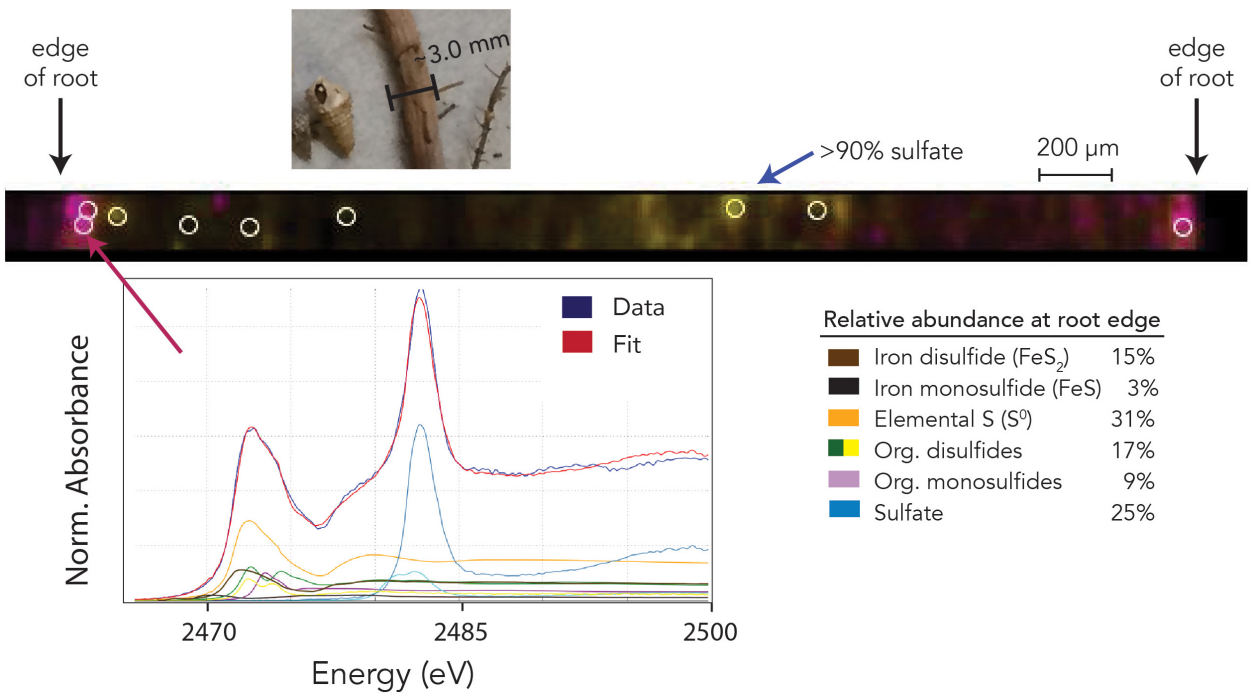

FIGURE 7 | Sulfur redox speciation across a transect of a ~3 mm mangrove root by X-ray fluorescence multi-energy mapping. The photo at top shows the root prior to splitting, with gastropods from bb10_R1 sediment. Map colors indicate the intensity (concentration) of sulfur at 2473 eV (pink, characteristic of various reduced forms) and 2482.3 eV (yellow, characteristic of sulfate). The pink color scale saturates at minimum and maximum values of 10–1000 counts (full data range = 0–1941 counts), and the yellow color scale ranges from 10 to 150 counts (full data range = 0–186 counts). White open circles show the locations at which full spectra were collected; the inset spectrum labeled "data" is an example for the outermost ~50 µm of the root, shown with its fitted components: iron mono- and disulfides, elemental S, sulfate, and organic (di)sulfides. Uncertainties from spectrum fitting (1σ) on listed relative abundances are ≤1%.

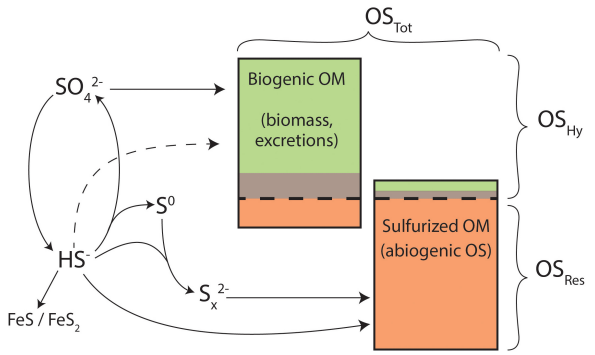

FIGURE 8 | Conceptual model for organic sulfur and its precursors in Little Ambergris Cay sediments. OS_{Tot} in mangrove sediments is composed of a mixture of biogenic and sulfurized OM (proportions not to scale), which derive sulfur from oxidized (SO_4) and reduced (HS^-, S_x^{2-}) sulfur forms. Potential direct assimilation of HS^- is shown as a dashed line. Potential iron sulfide formation via polysulfides is omitted for simplicity. Green, brown, and orange colors represent OS_{Hy} (moderate temp), OS_{Hy} (high temp), and OS_{Res} pools, as in **Figures 4**, **5**.

OM pool. The S-isotope composition of OS_{Hy} ranges from 9.5 to 20.0‰, approaching local seawater sulfate at 21.9‰ (Trower et al., 2018). Microbial primary producers assimilate seawater sulfate to synthesize S-bearing amino acids and other biochemicals (**Figure 8**), yielding fresh marine biomass with a similar $\delta^{34}S$ value (Kaplan and Rittenberg, 1964). Under some conditions, microbes can also assimilate environmental sulfide with a more ^{34}S-depleted composition (dashed line in **Figure 8**; Francois, 1987), but the size of this flux is poorly constrained. In clear contrast with OM_{Hy}, OS_{Res} is strongly ^{34}S-depleted and similar to concurrent inorganic S phases (**Figure 5**). OS_{Res}, S^0, and CRS all appear to derive their S from sulfide, which has a ^{34}S-depleted composition due to isotopic fractionation during microbial sulfate reduction (Kaplan and Rittenberg, 1964). In detail, the $\delta^{34}S$ value of OS_{Res} is consistently 3–5‰ more ^{34}S-enriched than coexisting S^0, even as the absolute $\delta^{34}S$ values of these pools differ (compare bb10_G3 and bb10_M in **Figure 5**). This 3–5‰ offset matches that observed experimentally between polysulfides (estimated from S^0) and sulfurized OM (Amrani and Aizenshtat, 2004). Plentiful S^0 in these sediments indicates that highly reactive polysulfides, which are thought to be primary reactants for both rapid OM sulfurization and pyrite formation (Kohnen et al., 1989; Amrani and Aizenshtat, 2004; Raven et al., 2016), were likely present in porewater (Rickard and Luther, 2007; Findlay and Kamyshny, 2017). The CRS pool, interpreted to primarily represent pyrite (Canfield et al., 1986), has $\delta^{34}S$ values matching those of S^0. Therefore, OS_{Res} likely formed from reactions with the same pool of polysulfides that precipitated S^0 and FeS_2. No contribution of biogenic S to OM_{Res} is required to explain its S-isotope composition.

Sulfur Sources and Speciation

Alkyl sulfides and disulfides are the major products of sulfurization in Little Ambergris Cay sediments, similar to observations from laboratory sulfurization experiments (Amrani and Aizenshtat, 2004), modern sites (Kohnen et al., 1991; Eglinton et al., 1994) and ancient rocks (Raven et al., 2018, 2019). At the same time, however, more oxidized forms are also significant contributors to OS_{Res} in these sediments. Sulfonates represent 23–25% of OS_{Res} in the bb10 gray surface mat and nearly that percentage throughout sample bb07; similar proportions were observed for shallow (<2 m sediment depth) Peru Margin sediments (Eglinton et al., 1994). Additionally, sulfate esters represent as much as 6.2% of OS_{Res} (in bb07_Sp2 and NBr) despite treatment with strong acid, which is generally expected to hydrolyze these structures. There are no obvious mixing relationships between the proportion of oxidized OS species in OS_{Res} and its S-isotope composition. Instead, OM_{Res} and S^0 $\delta^{34}S$ values in different samples are offset by a consistent amount, regardless of OS speciation (**Figure 5**). By implication, the oxidized OS structures in OM_{Res} appear to be sulfide-derived, resulting from either (1) OM sulfurization by (poly)sulfides, followed by later oxidation of organic sulfides to sulfonates (Gomez-Saez et al., 2016), or (2) sulfide oxidation to an intermediate species like sulfite, followed by subsequent reactions with OM to form sulfonates (Vairavamurthy et al., 1994).

The majority of OS_{Hy} is in the form of sulfate esters, at concentrations of up to 148 μmol S/g. These esters were measured after repeated washings with water and two, 30-min treatments with 1N HCl at room temperature, which will remove free sulfate salts but not hydrolyze ester-bound S (King and Klug, 1982). Sulfate esters are common in terrestrial, soil, and lake environments (King and Klug, 1982; David and Mitchell, 1985; Jokic et al., 2003; Prietzel et al., 2007) and are generally sourced from the aerobic biosphere: polysaccharides and excretions of animals, higher plants, and some algae (Fitzgerald, 1976). Abundant sulfate esters in Little Ambergris Cay push the S:C ratios of OM_{Hy} to as much as 3.9 mol%, ratios that are more typical of OM_{Res} from strongly sulfurized marine deposits and much higher than expected for biomass (Francois, 1987). In this system, potential sources for remarkably abundant sulfate esters include both mangrove plant exudates and products of benthic fauna like foraminifera, nematodes, and gastropods [historically used as a source of sulfate ester dyes (Scheuer, 1977)]. Due to the mismatch in C-isotopes between the plants and sediment OM (**Figure 4**, also discussed the following section), as well as the presence of plentiful esters in the root-free but gastropod-containing bb10 gray mat, excretions associated with macrofaunal digestion are the most likely sulfate ester source.

In addition to this pool of oxidized, hydrolyzable OS, ∼7–41% of the S in OM_{Hy} is reduced, in the form of sulfides and disulfides. Some of this contribution may simply illustrate the imperfect nature of our separation and could result from hydrolysis of OS_{Res}-like, abiotically sulfurized material. The lower-temperature portion of the OS_{Hy} pool was less strongly ^{34}S-depleted than the higher-temperature portion of OS_{Hy} (**Figure 5** and **Supplementary Table 1**), which would be consistent with some hydrolysis of (di)sulfides during the higher temperature treatment. Additionally, there is a moderately significant correlation (linear regression R^2 = 0.64, **Supplementary Figure 1**) between the proportion of alkyl

sulfides in OM_{Hy} and the $\delta^{34}S$ value of OM_{Hy}, which suggests mixing between a ^{34}S-rich, mostly oxidized OS pool and a more ^{34}S-depleted source. The y-intercept of this trendline (equivalent to the projected composition of purely oxidized OS) is 20.7‰, which is similar to the prediction for seawater sulfate-derived biomass [i.e., 18–22‰; (Kaplan and Rittenberg, 1964)]. Alternatively, some or all of the (di)sulfides in OM_{Hy} could represent small, hydrophilic S-bearing molecules that are released from association with higher-molecular-weight OM by acidification. For example, 3-mercaptopropionate, a product of the anaerobic degradation of dimethyl sulfoniopropionate (DMSP), is present at high concentrations in the tissue of certain salt marsh grasses and can bind to humic substances via di- or poly-sulfide linkages (Vairavamurthy et al., 1997). Although some disulfide bonds clearly persist after acidification (**Figure 6**), hydrolysis causes the loss of as much as 60 μmol disulfide S/g from the solid phase.

The acid hydrolysis-sequential extraction method used here is comparable to standard AVS and CRS techniques for separating organic and inorganic S pools in sediments. In marine and deep-time studies, the OS_{Hy} pool is frequently presumed to be minor and discarded. However, OS_{Hy} can be a significant pool of both C and S in environments that are rich in biomass, as seen both here as well as in sediments from Mangrove Bay, Bermuda, where OS_{Hy} is similarly abundant and ^{34}S-enriched below 10 cm depth (∼30 μmol S/g and 10–13‰) (Canfield et al., 1998).

Unlike Mangrove Bay, Little Ambergris Cay sediments do not contain large amounts of chromium-reducible organic S (CROS), which is thought to represent organic polysulfides in the solid phase (Canfield et al., 1998). As shown in **Figure 5**, CRS concentrations in Little Ambergris Cay sediments are consistently low and similar to estimated pyrite concentrations in pre-CRS sediments by XAS (**Supplementary Table 2**). Although some organic polysulfides could have been lost to oxidation from exposed surfaces of Little Ambergris Cay sediments during transport, S^0 concentrations are generally insufficient to account for the oxidation of a large organic polysulfide pool, and we find no evidence for $S \geq 3$ linkages in even the most interior parts of the sediment by XAS. Therefore, abundant organic polysulfides do not appear to be universal in mangrove sediments, and the controls on organic polysulfide formation relative to other forms of abiogenic OS remains an open question.

Carbon Sources, Fluxes, and Offset With Lipids

Throughout Little Ambergris Cay sediments, OM_{Tot} is distinctively ^{13}C-enriched (–13.7‰ ± 1.1‰) relative to typical inputs from mangrove plants ($\delta^{13}C \sim$ –28 to –30‰) or marine phytoplankton (–24 to –16‰). Similarly ^{13}C-enriched OM is common in microbial mats and is thought to result from CO_2 limitation within cyanobacterial mat layers, which causes reduced discrimination against ^{13}C during carbon fixation (Calder and Parker, 1973; Houghton et al., 2014). Therefore, CO_2-limited benthic mats are the dominant source of organic carbon to both OM_{Res} and OM_{Hy}, and the fibrous structures in dark brown bb10 sediments, termed "micro-roots" (**Supplementary Table 1**), are not likely to be a large contribution to biomass. Slightly more ^{13}C-depleted OM in a root-adjacent sample (R1) and both "peaty" samples from bb07 (∼ –15.2‰) could reflect a larger albeit still minor contribution from ^{13}C-depleted, plant-derived OM in these regions. Nonetheless, the flux of mangrove-derived carbon to sedimentary OM_{Tot} in Little Ambergris Cay is small (Gomes et al., 2016).

The S:C ratios of OM_{Res} at this site are quite low relative to strongly sulfurized marine sites (S:C ≤ 8%; Raiswell et al., 1993; Raven et al., 2019), with a maximum value of only 1.2 mol% (in bb10_R1) and typical values closer to 0.6 mol%. In the latter case, this means that OM_{Res} contains 167 C atoms for every added S, far more than can be causally linked to preservation due to a single sulfurization event. The amount of C that can be effectively preserved for each sulfur addition has been estimated at roughly 8–30 C atoms (Raven et al., 2018). Accordingly, in a sample with an S:C ratio of 0.6 mol%, OM sulfurization (as a mechanism for enhancing hydrolysis resistance) accounts for essentially all of the S in OM_{Res} but only 5–18% of the C. The remainder of C in OM_{Res} represents OM that is naturally hydrolysis resistant, ^{13}C-enriched, and S-poor. Likely sources of this material are the degradation products of extracellular polymeric substances (EPS), which are a blend of carbohydrates, lipids, and other components, and/or the polysaccharide sheaths from cyanobacteria in the surface mat (Underwood et al., 2004; Flemming et al., 2007). In sum, OM_{Res} in Little Ambergris Cay sediment is a mixture of sulfurization products and naturally hydrolysis-resistant, S-poor OM, potentially related to EPS from benthic microbial mats.

OM_{Res} is consistently more ^{13}C-depleted than OM_{Hy}, with a $\delta^{13}C$ difference of 2.6–5.3‰ (**Figure 4** and **Table 1**). One likely contributor to this offset is the difference in C-isotope compositions between lipids and carbohydrates. Lipids, which are naturally hydrolysis-resistant and easily sulfurizable (Sinninghe Damsté et al., 1988) are also generally ^{13}C-depleted relative to bulk biomass due to kinetic isotope effects associated with their biosynthesis. Carbohydrates, on the other hand, are typically more ^{13}C-enriched than bulk biomass (Hayes, 2001). The size of the isotopic offset between carbohydrates and lipids depends on the organism and on the details of biosynthetic fluxes within the cell: in a survey of aquatic and terrestrial plants, the offset between glucose and fatty acids ranged from ∼3 to 16‰ (van Dongen et al., 2002). This effect could be sufficient to explain the $\delta^{13}C$ differences we observe between OM_{Hy} and OM_{Res}, if lipids preferentially constitute OM_{Res} while carbohydrates or "bulk biomass" constitute OM_{Hy}. Additionally, the $\delta^{13}C$ offset could be enhanced by trophic enrichment of heterotrophically processed biomass in OM_{Hy} (e.g., gastropod excretions) relative to OM_{Res} (e.g., EPS generated by cyanobacteria).

Spatial Patterns of Sulfur Cycling Near Mangrove Roots

The extent of OM sulfurization varies spatially in Little Ambergris Cay sediments. The most strongly sulfurized OM in sediment, indicated by the highest OM_{Res} S:C ratios and the highest proportion of sulfides, is located in a 1–2 cm zone

surrounding the 3-mm-diameter bb10 root (bb10_R). These locations are also associated with elevated concentrations of OM_{Res}, S^0, and CRS, indicating enhanced rates of sedimentary S cycling in the immediate vicinity of the root. A cascade of redox reactions among O_2, OM, Fe, and S species may be initiated by a flux of O_2 from mangrove roots (Thibodeau and Nickerson, 1986), as certain mangrove species actively oxygenate their root environment to improve their tolerance to waterlogged, anaerobic conditions ("Radial Oxygen Loss"; Armstrong, 1980), which significantly impacts local sediment geochemistry (Nickerson and Thibodeau, 1985). Parts of a mangrove root system have been shown to transport O_2 from pneumatophores to root tips with minimal leakage (Andersen and Kristensen, 1988); the woody trunk material in sample bb07 may represent this type of O_2-transporting structure. Near the tips of actively growing roots, translocated O_2 is released at measured rates on the order of 1–10 μmol O/cm^2/day (Pi et al., 2010). At these approximate rates, the 5-cm-long, 3-mm-diameter bb10 root would generate 1.8–18 μmol O_2/day; for comparison, region bb10_R contains a total of 81 μmols of S^0.

The outermost 50 μm or so of the bb10 root surface also hosts a significant amount of solid-phase S – equivalent to ∼2.4 wt% of dry root mass. This S seems to have a splotchy distribution (**Figure 7**), which could result either from uneven microbial communities on the root surface, or from heterogeneity in root O_2 release (Pi et al., 2010). The S-isotope composition of the root surface averages to approximately –21‰, very similar to OS_{Res} in adjacent sediment (bb10_R, averaging –22.5‰). Accordingly, reduced S phases in the root surface appear to derive from the same pool of dissolved (poly)sulfide as surrounding sedimentary OS_{Res} and FeS_2.

The organic S in the root cortex has a distinctly different speciation from that in the immediately surrounding sediments. We find no evidence for more oxidized OS moieties like sulfonates or sulfate esters in the root cortex. Additionally, the root cortex has a much greater degree of S–S bonding than the surrounding sediments, indicating that these locations host distinct types of potential S reactivity. The high concentrations of apparent disulfides and S^0 that we observe in the root cortex could potentially represent organic polysulfides, which contain zero-valent S atoms that appear as S^0 by XAS as well as S–S bonds with a disulfide character. Whether zero-valent S^0 is present primarily as organic polysulfides or as a solid or nano-particulate phase, it is expected to significantly affect the favorability of abiotic reaction mechanisms (e.g., Avetisyan et al., 2019) and microbial metabolisms (e.g., Findlay, 2016) at this interface.

In the absence of local terrestrial weathering, the primary source of Fe to Little Ambergris Cay is likely to be wind-blown dust from Saharan West Africa (Maloof et al., 2007). Approximately 18% of the S in the root cortex is bound to Fe, either as FeS or FeS_2. This represents a slight concentration of Fe on the root surface relative to surrounding sediments, where CRS and AVS together represent 12–17% of "sulfide-derived" S (OS_{Res} + S^0 + AVS + CRS) or ∼5% of total solid-phase S (including OS_{Hy}). In all other sediment samples, Fe phases represent an average of 9% of sulfide-derived S (1.8% of total S). Fe is known to accumulate on the surfaces of O_2-pumping roots, especially under strongly anaerobic conditions (e.g., wastewater treatment scenarios). Roots frequently develop a "plaque" of iron oxides on their surfaces due to the oxidation of Fe^{2+} ions with O_2 (Hansel et al., 2001; Pi et al., 2010), which can effectively exclude Fe, Zn, and other potentially toxic metals from the xylem (Machado et al., 2005). Root-surface iron oxides could serve as a substrate for microbial Fe reduction under fluctuating redox conditions and support the formation of FeS_2 on and/or near the root surface (Holmer et al., 1994; Sherman et al., 1998). FeS_2 could be thus be a significant component of root plaque under strongly reducing conditions and perhaps act as a barrier to further oxygenation of the rhizosphere. Root-mediated Fe cycling may also lead to elevated Fe concentrations in bb10_R (6.7 and 9.5 μmol Fe/g, assuming a 1:2 Fe:S stoichiometry for CRS) relative to other regions of the sediment.

Within the vascular tissues, S is composed of >90% sulfate with smaller, less-well-constrained amounts of S^0 and reduced organic S. S in the root xylem has a $\delta^{34}S$ value of –7.2‰, almost 30‰ more ^{34}S-depleted than seawater sulfate (21‰). Given its isotopic composition, the most probable source of this ^{34}S-depleted sulfate is sulfide oxidation, followed by mixing with seawater sulfate. Similar $\delta^{34}S$ values have been reported from mangrove leaves, which led authors to propose that mangroves actively assimilated and/or oxidized sulfide, potentially to reduce their sulfide exposure (Fry et al., 1982; Canfield et al., 1998). Our results thus indicate that mangroves do oxidize sulfide, either directly (e.g., enzymatically) or indirectly (e.g., by releasing O_2) resulting in ^{34}S-depleted sulfate in their root vascular tissues.

Interactions With Macrofauna

Paradoxically, Little Ambergris Cay sediments are rich in both sulfurized OM, suggesting sulfidic conditions, and gastropods, suggesting oxic conditions. Observed gastropods are likely to be *Cerithidea obtusa*, which favor consumption of benthic microalgae over plant litter (Bouillon et al., 2002). The collective impact of macrofauna activity on marine sediments is broadly to reduce OM preservation, at least on decadal timescales (Middelburg and Levin, 2009; Lichtschlag et al., 2015; Jessen et al., 2017), and to support Fe^{III}-cycling metabolisms during oxic sediment reworking (Thamdrup, 2000; Nielsen et al., 2003; Kristensen and Alongi, 2006). However, gastropods have only a limited tolerance for sulfidic conditions, which stymie their growth and reproduction (Aguirre-Velarde et al., 2018). Gastropods were remarkably abundant (>21 wt%) in bb10_M and somewhat less so (2–8 wt%) in other parts of sample bb10. Although we cannot rule out the presence of deceased gastropods that fell into the mat, these spatial patterns differ than what would by predicted by chance trapping of the gastropods in sediment. Despite abundant S^0 and OS_{Res} in bb10_M and B, which attest to the activity of microbial sulfate reduction in these samples, gastropods in these same sediments are clearly able to access sufficient O_2 for their metabolism.

Spatial gradients could allow for the concurrence of porewater sulfide and macrofauna if the sources and sinks for sulfide are localized within μm- to mm-scale microenvironments in sediment aggregates. Sulfide production and precipitation on this

length-scale could co-exist with sufficient O_2 in larger pore spaces to allow for macrofauna respiration. Alternatively, diurnal or tidal redox cycles could explain the coexistence of macrofauna and sulfurization. Gastropods tolerate recurrent sulfide exposure on the Peru Margin, although it comes at a significant metabolic and reproductive cost (Levin et al., 2009; Aguirre-Velarde et al., 2018). As a final option, the gastropods may have populated oxic sediments that were exposed to sulfide during a previous year or season. Porewater sulfide measurements in future work will help discern among these options.

Impact of Sulfurization on Carbon Burial

In the specific case of Little Ambergris Cay, it is challenging to meaningfully assess the contribution of sulfurization to long-term carbon burial because recurrent storms at this site cause physical erosion and episodically remove accumulated material (Wanless and Dravis, 2008). Still, the gray surface mat (bb10_G) appears to be representative of the OM source to underlying sediments (bb10_B, M, and R), which all show evidence for OM sulfurization. The molar S:C ratio of OM_{Res} increases from an average of 0.5% in the mat to an average of 1.1% in bb10_B, M, and R; and, there is a roughly two-fold increase in the average carbonate–free concentration of OS_{Res} between the gray mat (90 μmol/g) and bb10_B, M, and R (201 μmol/g). This pattern suggests that OM sulfurization below the benthic mat leads to an approximate doubling in the amount of OS_{Res} and, using the estimated stoichiometry of 8–30 C atoms preserved for each abiogenic OS atom, the additional potential preservation of 0.35–1.3 mmol C/g sediment (2.5–9.2 mmol C/g carbonate-free sediment).

Contrasting marine systems, OM sulfurization in coastal ecosystems occurs under more heterogeneous and dynamic conditions, where oxidant availability is not controlled by a simple one-dimensional diffusive gradient at the sediment-water interface (Nedwell et al., 1994; Pan et al., 2018). Instead, the local redox state in the sediments is likely variable, responding to diurnal cycles in photosynthetic activity and tidal inundation as well as local sources of O_2 from roots. There is significant evidence for biogeochemical S cycling and OM sulfurization in the sediments even within the cohesive gray surface mat (bb10_G), indicating that long-term (kyr) incubation with dissolved sulfide is not driving the observed sulfurization. Instead, rapid reactions between polysulfides and functionalized, likely lipid-rich biomass generate OM with a very high resistance to hydrolysis, enhancing the potential long-term preservation of microbially reduced carbon and sulfur in the geosphere. OM sulfurization is likely active in a variety of coastal and marginal settings that experience intermittent sedimentary anoxia and may be a critical mechanism impacting carbon cycling in many coastal OM burial hotspots.

CONCLUSION

Organic matter sulfurization is widespread in Little Ambergris Cay sediments with a variety of textures, including structured microbial mats, spongey brown sediments with mm-scale roots, and ooid-dominated sands surrounding woody trunks. OM sulfurization is most extensive on and near the surface of a O_2-releasing root, where it co-occurs with plentiful elemental S^0 and indicates enhanced local microbial sulfur cycling. Overall, these data thus support the hypothesis that radial oxygen loss from mangroves enhances local OM preservation by facilitating biogeochemical sulfur cycling.

Carbon preservation in mangrove sediments has the potential to respond to small-scale heterogeneities in redox state and the availability of OM, metals, O_2, and H_2S. Understanding the competition among sulfide sinks at the sediment-root interface will be critical for modeling overall environmental rates of OM remineralization vs. OM sulfurization. OM sulfurization in mangroves is not typically accounted for in regional or global carbon budgets, which instead attribute non-mangrove carbon burial to allochthonous sources (e.g., terrestrial runoff). However, as illustrated in Little Ambergris Cay, sulfurization has the potential to be a major control on the storage of microbially derived OM in mangrove ecosystems. Understanding the scale and sensitivities of this flux will require further investigations into the small-scale redox gradients and critical hotspots for reactivity associated with mangrove roots.

AUTHOR CONTRIBUTIONS

MR and MG designed the study. MG conducted the fieldwork. MR prepared and analyzed the samples, evaluated the geochemical data, and drafted the manuscript. SW and MR collected and analyzed the X-ray data. MR, MG, and DF interpreted the data and developed the conclusions. All authors contributed to the final manuscript.

FUNDING

This work was financially supported by the Agouron Institute through the Geobiology Postdoctoral Fellowship to MR. Travel and sampling support were provided by the Agouron Institute through the Advanced Geobiology Course led by John Grotzinger (California Institute of Technology) and Andrew Knoll (Harvard University). This work was enhanced by XAS analyses at the Stanford Synchrotron Radiation Laboratory under User Proposal 4885 to MR and DF. Use of the Stanford Synchrotron Radiation Lightsource, SLAC National Accelerator Laboratory, is supported by the U.S. Department of Energy, Office of Science, Office of Basic Energy Sciences under Contract No. DE-AC02-76SF00515.

ACKNOWLEDGMENTS

We are grateful to the Department of Environment and Coastal Resources (DECR), Turks and Caicos Island Government for granting a research permit to perform this work to John Grotzinger. We also thank participants, the Advanced Geobiology Course, Roger Tarika, Bevo Tarika, Paul Mahoney, James Seymour and the support staff on Big Ambergris Cay for their logistical support. We thank Derek Smith for valuable

discussions during project conception, Alex Bradley for the use of his lab facility, and Melanie Suess, Jen Houghton, and Stephanie Moore for analytical support at Washington University in St. Louis. We also thank G. Gomez-Saez and A. Kamyshny for constructive and helpful reviews.

SUPPLEMENTARY MATERIAL

The Supplementary Material for this article can be found online at: https://www.frontiersin.org/articles/10.3389/feart.2019.00098/full#supplementary-material

REFERENCES

Aguirre-Velarde, A., Pecquerie, L., Jean, F., Thouzeau, G., and Flye-Sainte-Marie, J. (2018). Predicting the energy budget of the scallop argopecten purpuratus in an oxygen–limiting environment. *J. Sea Res.* 143, 254–261. doi: 10.1016/j.seares.2018.09.011

Alongi, D. M. (2014). Carbon cycling and storage in mangrove forests. *Annu. Rev. Mar. Sci.* 6, 195–219. doi: 10.1146/annurev-marine-010213-135020

Amrani, A., and Aizenshtat, Z. (2004). Mechanisms of sulfur introduction chemically controlled: δ34S imprint. *Org. Geochem.* 35, 1319–1336. doi: 10.1016/j.orggeochem.2004.06.019

Andersen, F. O., and Kristensen, E. (1988). The influence of macrofauna on estuarine benthic community metabolism: a microcosm study. *Mar. Biol.* 99, 591–603. doi: 10.1007/bf00392566

Armstrong, W. (1980). "*Aeration in higher plants*," in *Advances in Botanical Research*, ed. J. A. Callow (Amsterdam: Elsevier), 225–332. doi: 10.1016/s0065-2296(08)60089-0

Arnosti, C., Bell, C., Moorhead, D. L., Sinsabaugh, R. L., Steen, A. D., Stromberger, M., et al. (2014). Extracellular enzymes in terrestrial, freshwater, and marine environments: perspectives on system variability and common research needs. *Biogeochemistry* 117, 5–21. doi: 10.1007/s10533-013-9906-5

Avetisyan, K., Buchshtav, T., and Kamyshny, A. Jr. (2019). Kinetics and mechanism of polysulfides formation by a reaction between hydrogen sulfide and orthorhombic cyclooctasulfur. *Geochim. Cosmochim. Acta* 247, 96–105. doi: 10.1016/j.gca.2018.12.030

Boudreau, B. P., Canfeld, D. E., and Mucci, A. (1992). Early diagenesis in a marine sapropel, Mangrove Lake, Bermuda. *Limnol. Oceanogr.* 37, 1738–1753. doi: 10.4319/lo.1992.37.8.1738

Bouillon, S., Koedam, N., Raman, A., and Dehairs, F. (2002). Primary producers sustaining macro-invertebrate communities in intertidal mangrove forests. *Oecologia* 130, 441–448. doi: 10.1007/s004420100814

Boussafir, M., Gelin, F., Lallier-Verges, E., Derenne, S., Bertrand, P., and Largeau, C. (1995). Electron microscopy and pyrolysis of kerogens from the Kimmeridge Clay Formation, UK: source organisms, preservation processes, and origin of microcycles. *Geochim. Cosmochim. Acta* 59, 3731–3747. doi: 10.1016/0016-7037(95)00273-3

Brassell, S. C., Lewis, C. A., De Leeuw, J. W., de Lange, F., and Damste, J. S. (1986). Isoprenoid thiophenes: novel products of sediment diagenesis? *Nature* 320, 160–162. doi: 10.1038/320160a0

Burdige, D. J. (2007). Preservation of organic matter in marine sediments: controls, mechanisms, and an imbalance in sediment organic carbon budgets? *Chem. Rev.* 107, 467–485. doi: 10.1021/cr050347q

Burton, E. D., Sullivan, L. A., Bush, R. T., Johnston, S. G., and Keene, A. F. (2008). A simple and inexpensive chromium-reducible sulfur method for acid-sulfate soils. *Appl. Geochem.* 23, 2759–2766. doi: 10.1016/j.apgeochem.2008.07.007

Calder, J. A., and Parker, P. L. (1973). Geochemical implications of induced changes in C13 fractionation by blue-green algae. *Geochim. Cosmochim. Acta* 37, 133–140. doi: 10.1016/0016-7037(73)90251-2

Canfield, D. E., Boudreau, B. P., Mucci, A., and Gundersen, J. K. (1998). The early diagenetic formation of organic sulfur in the sediments of Mangrove Lake, Bermuda. *Geochim. Cosmochim. Acta* 62, 767–781. doi: 10.1016/s0016-7037(98)00032-5

Canfield, D. E., Raiswell, R., Westrich, J. T., and Reaves, C. M. (1986). The use of chromium reduction in the analysis of reduced inorganic sulfur in sediments and shales. *Chem. Geol.* 54, 149–155. doi: 10.1016/0009-2541(86)90078-1

Chróst, R. J. (1991). "*Environmental control of the synthesis and activity of aquatic microbial ectoenzymes*," in *Microbial Enzymes in Aquatic Environments Brock/Springer Series in Contemporary Bioscience*, ed. C. Ryszard (New York, NY : Springer).

David, M. B., and Mitchell, M. J. (1985). Sulfur constituents and cycling in waters, seston, and sediments of an oligotrophic lake. *Limnol. Oceanogr.* 30, 1196–1207. doi: 10.4319/lo.1985.30.6.1196

Duarte, C. M., and Prairie, Y. T. (2005). Prevalence of heterotrophy and atmospheric CO2 emissions from aquatic ecosystems. *Ecosystems* 8, 862–870. doi: 10.1007/s10021-005-0177-4

Eglinton, T. I., Irvine, J. E., Vairavamurthy, A., Zhou, W., and Manowitz, B. (1994). Formation and diagenesis of macromolecular organic sulfur in Peru margin sediments. *Organ. Geochem.* 22, 781–799. doi: 10.1016/0146-6380(94)90139-2

Ellison, J., and Zouh, I. (2012). Vulnerability to climate change of mangroves: assessment from Cameroon, Central Africa. *Biology* 1, 617–638. doi: 10.3390/biology1030617

Findlay, A. J. (2016). Microbial impact on polysulfide dynamics in the environment. *FEMS Microbiol. Lett.* 363:fnw103. doi: 10.1093/femsle/fnw103

Findlay, A. J., and Kamyshny, A. (2017). Turnover rates of intermediate sulfur species (Sx2-, S0, S2O32-, S4O62-, SO32-) in anoxic freshwater and sediments. *Front. Microbiol.* 8:2551. doi: 10.3389/fmicb.2017.02551

Fitzgerald, J. W. (1976). Sulfate ester formation and hydrolysis: a potentially important yet often ignored aspect of the sulfur cycle of aerobic soils. *Bacteriol. Rev.* 40, 698–721.

Flemming, H. C., Neu, T. R., and Wozniak, D. J. (2007). The EPS matrix: the "House of Biofilm Cells.". *J. Bacteriol.* 189, 7945–7947. doi: 10.1128/jb.00858-07

Francois, R. (1987). A study of sulphur enrichment in the humic fraction of marine sediments during early diagenesis. *Geochim. Cosmochim. Acta* 51, 17–27. doi: 10.1016/0016-7037(87)90003-2

Fry, B., Scalan, R. S., Winters, J. K., and Parker, P. L. (1982). Sulphur uptake by salt grasses, mangroves, and seagrasses in anaerobic sediments. *Geochim. Cosmochim. Acta* 46, 1121–1124. doi: 10.1016/0016-7037(82)90063-1

Gilman, E. L., Ellison, J., Duke, N. C., and Field, C. (2008). Threats to mangroves from climate change and adaptation options: a review. *Aquat. Bot.* 89, 237–250. doi: 10.1016/j.aquabot.2007.12.009

Gomes, M. L., Lingappa, U., Metcalfe, K., O'Reilly, S. S., Riedman, L. A., Cantine, M., et al. (2016). *Linking the Modern to the Ancient With A Comprehensive Geobiological Understanding of Biosignature Preservation in Microbial Mats*. Washington, DC: American Geochemical Union Fall Meeting,

Gomez-Saez, G. V., Niggemann, J., Dittmar, T., Pohlabeln, A. M., Lang, S. Q., Noowong, A., et al. (2016). Molecular evidence for abiotic sulfurization of dissolved organic matter in marine shallow hydrothermal systems. *Geochim. Cosmochim. Acta* 190, 35–52. doi: 10.1016/j.gca.2016.06.027

Hansel, C. M., Fendorf, S., Sutton, S., and Newville, M. (2001). Characterization of Fe plaque and associated metals on the roots of mine-waste impacted aquatic plants. *Environ. Sci. Technol.* 35, 3863–3868. doi: 10.1021/es0105459

Hayes, J. M. (2001). "Fractionation of the isotopes of carbon and hydrogen in biosynthetic processes," in *Proceedings of the National Meeting of the Geological Society of America*, Boston, MA.

Hebting, Y., Schaeffer, P., Behrens, A., Adam, P., Schmitt, G., Schneckenburger, P., et al. (2006). Biomarker evidence for a major preservation pathway of sedimentary organic carbon. *Science* 312, 1627–1631. doi: 10.1126/science.1126372

Holmer, M., Kristensen, E., Banta, G., Hansen, K., Jensen, M., and Bussawarit, N. (1994). Biogeochemical cycling of sulfur and iron in sediments of a south-east Asian mangrove, Phuket Island, Thailand. *Biogeochemistry* 26, 145–161.

Houghton, J., Fike, D., Druschel, G., Orphan, V., Hoehler, T. M., and Marais Des, D. J. (2014). Spatial variability in photosynthetic and heterotrophic activity drives localized $\delta^{13}C_{org}$ fluctuations and carbonate precipitation in hypersaline microbial mats. *Geobiology* 12, 557–574. doi: 10.1111/gbi.12113

Hulthe, G., Hulth, S., and Hall, P. (1998). Effect of oxygen on degradation rate of refractory and labile organic matter in continental margin sediments. *Geochim. Cosmochim. Acta* 62, 1319–1328. doi: 10.1016/s0016-7037(98)00044-1

Jennerjahn, T. C., and Ittekkot, V. (2004). Relevance of mangroves for the production and deposition of organic matter along tropical continental margins. *Naturwissenschaften* 89, 23–30. doi: 10.1007/s00114-001-0283-x

Jessen, G. L., Lichtschlag, A., Ramette, A., Pantoja, S., Rossel, P. E., Schubert, C. J., et al. (2017). Hypoxia causes preservation of labile organic matter and changes seafloor microbial community composition (Black Sea). *Sci. Adv.* 3:e1601897. doi: 10.1126/sciadv.1601897

Jokic, A., Cutler, J. N., Ponomarenko, E., van der Kamp, G., and Anderson, D. W. (2003). Organic carbon and sulphur compounds in wetland soils: insights on structure and transformation processes using K-edge XANES and NMR spectroscopy. *Geochim. Cosmochim. Acta* 67, 2585–2597. doi: 10.1016/s0016-7037(03)00101-7

Jorgensen, B. B. (1982). Mineralization of organic matter in the sea bed-the role of sulphate reduction. *Nature* 296, 643–645. doi: 10.1038/296643a0

Kaplan, I. R., and Rittenberg, S. C. (1964). Microbiological fractionation of sulphur isotopes. *J. Gen. Microbiol.* 34, 195–212. doi: 10.1099/00221287-34-2-195

King, G. M., and Klug, M. J. (1982). Comparative aspects of sulfur mineralization in sediments of a Eutrophic Lake Basin. *Appl. Environ. Microbiol.* 43, 1406–1412.

Kohnen, M., Damste, J. S., Haven ten, H. L., and De Leeuw, J. W. (1989). Early incorporation of polysulfides in sedimentary organic matter. *Nature* 341, 640–641. doi: 10.1038/341640a0

Kohnen, M., Sinninghe, J. S. D., Dalen, A. K.-V., and De Leeuw, J. W. (1991). Di- or polysulphide-bound biomarkers in sulphur-rich geomacromolecules as revealed by selective chemolysis. *Geochim. Cosmochim. Acta* 55, 1375–1394. doi: 10.1016/0016-7037(91)90315-v

Kristensen, E., Ahmed, S. I., and Devol, A. H. (1995). Aerobic and anaerobic decomposition of organic matter in marine sediment: which is fastest? *Limnol. Oceanogr.* 40, 1430–1437. doi: 10.4319/lo.1995.40.8.1430

Kristensen, E., and Alongi, D. (2006). Control by fiddler crabs *(Uca vocans)* and plant roots *(Avicennia marina)* on carbon, iron, and sulfur biogeochemistry in mangrove sediment. *Limnol. Oceanogr.* 51, 1557–1571. doi: 10.4319/lo.2006.51.4.1557

Kristensen, E., Bouillon, S., Dittmar, T., and Marchand, C. (2008). Organic carbon dynamics in mangrove ecosystems: a review. *Aquat. Bot.* 89, 201–219. doi: 10.1016/j.aquabot.2007.12.005

Levin, L. A., Ekau, W., Gooday, A. J., Jorissen, F., Middelburg, J. J., Naqvi, S. W. A., et al. (2009). Effects of natural and human-induced hypoxia on coastal benthos. *Biogeosciences* 6, 2063–2098. doi: 10.5194/bg-6-2063-2009

Lichtschlag, A., Donis, D., Janssen, F., Jessen, G. L., Holtappels, M., Wenzhöfer, F., et al. (2015). Effects of fluctuating hypoxia on benthic oxygen consumption in the Black Sea (Crimean Shelf). *Biogeosci. Discuss.* 12, 6445–6488. doi: 10.5194/bgd-12-6445-2015

Lovelock, C. E., Cahoon, D. R., Friess, D. A., Guntenspergen, G. R., Krauss, K. W., Reef, R., et al. (2015). The vulnerability of Indo-Pacific mangrove forests to sea-level rise. *Nature* 526, 559–563. doi: 10.1038/nature15538

Luther, G. W. III, Glazer, B. T., Hohmann, L., Popp, J. I., Taillefert, M., Rozan, T. F., et al. (2001). Sulfur speciation monitored in situ with solid state gold amalgam voltammetric microelectrodes: polysulfides as a special case in sediments, microbial mats and hydrothermal vent waters. *J. Environ. Monitor.* 3, 61–66. doi: 10.1039/b006499h

Machado, W., Gueiros, B. B., Lisboa-Filho, S. D., and Lacerda, L. D. (2005). Trace metals in mangrove seedlings: role of iron plaque formation. *Wetl. Ecol. Manage.* 13, 199–206. doi: 10.1007/s11273-004-9568-0

Maloof, A. C., Kopp, R. E., Grotzinger, J. P., Fike, D. A., Bosak, T., Vali, H., et al. (2007). Sedimentary iron cycling and the origin and preservation of magnetization in platform carbonate muds, Andros Island, Bahamas. *Earth Planet. Sci. Lett.* 259, 581–598. doi: 10.1016/j.epsl.2007.05.021

Mazda, Y., and Ikeda, Y. (2006). Behavior of the groundwater in a riverine-type mangrove forest. *Wetl. Ecol. Manage.* 14, 477–488. doi: 10.1007/s11273-006-9000-z

Middelburg, J. J., and Levin, L. A. (2009). Coastal hypoxia and sediment biogeochemistry. *Biogeosciences* 6, 1273–1293. doi: 10.5194/bg-6-1273-2009

Nedwell, D. B., Blackburn, T. H., and Wiebe, W. J. (1994). Dynamic nature of the turnover of organic carbon, nitrogen and sulphur in the sediments of a Jamaican mangrove forest. *Mar. Ecol. Prog. Ser.* 110, 223–231. doi: 10.3354/meps110223

Nickerson, N. H., and Thibodeau, F. R. (1985). Association between pore water sulfide concentrations and the distribution of mangroves. *Biogeochemistry* 1, 183–192. doi: 10.1007/bf02185041

Nielsen, O. L., Kristensen, E., and Macintosh, D. J. (2003). Impact of fiddler crabs (Uca spp.) on rates and pathways of benthic mineralization in deposited mangrove shrimp pond waste. *J. Exp. Mar. Biol. Ecol.* 289, 59–81. doi: 10.1016/s0022-0981(03)00041-8

Orzechowski, E. A., Strauss, J. V., Knoll, A. H., Fischer, W. W., Cantine, M., Metcalfe, K., et al. (2016). *Age and Construction of Little Ambergris Cay Bedrock Rim, Southeastern Caicos Platform, British West Indies*. Washington, DC: American Geophysical Union Fall Meeting .

Pan, F., Liu, H., Guo, Z., Li, Z., Wang, B., Cai, Y., et al. (2018). Effects of tide and season changes on the iron-sulfur-phosphorus biogeochemistry in sediment porewater of a mangrove coast. *J. Hydrol.* 568, 686–702. doi: 10.1016/j.jhydrol.2018.11.002

Pi, N., Tam, N. F. Y., and Wong, M. H. (2010). Effects of wastewater discharge on formation of Fe plaque on root surface and radial oxygen loss of mangrove roots. *Environ. Pollut.* 158, 381–387. doi: 10.1016/j.envpol.2009.09.004

Prietzel, J., Thieme, J., Salome, M., and Knicker, H. (2007). Sulfur K-edge XANES spectroscopy reveals differences in sulfur speciation of bulk soils, humic acid, fulvic acid, and particle size separates. *Soil Biol. Biochem.* 39, 877–890. doi: 10.1016/j.soilbio.2006.10.007

Raiswell, R., Bottrell, S. H., Al-Biatty, A. J., and Tan, M. (1993). The influence of bottom water oxygenation and reactive iron content on sulfur incorporation into bitumens from Jurassic marine shales. *Am. J. Sci.* 293, 569–596. doi: 10.2475/ajs.293.6.569

Raven, M. R., Fike, D. A., Bradley, A. S., Gomes, M. L., Owens, J. D., and Webb, S. A. (2019). Paired organic matter and pyrite δ34S records reveal mechanisms of carbon, sulfur, and iron cycle disruption during Ocean Anoxic Event 2. *Earth Planet. Sci. Lett.* 512, 27–38. doi: 10.1016/j.epsl.2019.01.048

Raven, M. R., Fike, D. A., Gomes, M. L., Webb, S. M., Bradley, A. S., and McClelland, H.-L. O. (2018). Organic carbon burial during OAE2 driven by changes in the locus of organic matter sulfurization. *Nat. Commun.* 9:3409. doi: 10.1038/s41467-018-05943-6

Raven, M. R., Sessions, A. L., Adkins, J. F., and Thunell, R. C. (2016). Rapid organic matter sulfurization in sinking particles from the Cariaco Basin water column. *Geochim. Cosmochim. Acta* 190, 175–190. doi: 10.1016/j.gca.2016.06.030

Rickard, D., and Luther, G. W. (2007). Chemistry of iron sulfides. *Chem. Rev.* 107, 514–562. doi: 10.1021/cr0503658

Scheuer, P. J. (1977). The varied and fascinating chemistry of marine mollusks. *Isr. J. Chem.* 16, 52–56. doi: 10.1002/ijch.197700012

Sherman, R. E., Fahey, T. J., and Howarth, R. W. (1998). Soil-plant interactions in a neotropical mangrove forest: iron, phosphorus and sulfur dynamics. *Oecologia* 115, 553–563. doi: 10.1007/s004420050553

Sinninghe Damsté, J. S., Irene, W., Rijpstra, C., De Leeuw, J. W., and Schenck, P. A. (1988). Origin of organic sulphur compounds and sulphur-containing high molecular weight substances in sediments and immature crude oils. *Organ. Geochem.* 13, 593–606. doi: 10.1016/0146-6380(88)90079-4

Stein, N., Quinn, D. P., Grotzinger, J. P., Fischer, W. W., Knoll, A. H., Cantine, M., et al. (2016). *UAV, GDPS, and Laser Transit Mapping of Microbial Mat Ecosystems on Little Ambergris Cay, BWI*. Washington, DC: American Geophysical Union Fall Meeting.

Thamdrup, B. (2000). Bacterial manganese and iron reduction in aquatic sediments. *Adv. Microb. Ecol.* 16, 41–84. doi: 10.1007/978-1-4615-4187-5_2

Thibodeau, F. R., and Nickerson, N. H. (1986). Differential oxidation of mangrove substrate by *Avicennia germinans* and *Rhizophora mangle*. *Am. J. Bot.* 73, 512–516. doi: 10.1002/j.1537-2197.1986.tb12069.x

Trembath-Reichert, E., Ward, L. M., Slotznick, S. P., Bachtel, S. L., Kerans, C., Grotzinger, J. P., et al. (2016). Gene sequencing-based analysis of microbial-mat morphotypes, Caicos platform, British West Indies. *J. Sediment. Res.* 86, 629–636. doi: 10.2110/jsr.2016.40

Trower, E. J., Cantine, M. D., Gomes, M. L., Grotzinger, J. P., Knoll, A. H., Lamb, M. P., et al. (2018). Active ooid growth driven by sediment transport in a high-energy shoal, Little Ambergris Cay, Turks and Caicos Islands. *J. Sediment. Res.* 88, 1132–1151. doi: 10.2110/jsr.2018.59

Twilley, R. R., Chen, R. H., and Hargis, T. (1992). Carbon sinks in mangroves and their implications to carbon budget of tropical coastal ecosystems. *Water Air Soil Pollut.* 64, 265–288. doi: 10.1007/978-94-011-2793-6_15

Underwood, G., Boulcott, M., Raines, C. A., and Waldron, K. (2004). Environmental effects on exopolymer production by marine benthic diatoms: dynamics, changes in composition, and pathways of production. *J. Phycol.* 40, 293–304. doi: 10.1111/j.1529-8817.2004.03076.x

Vairavamurthy, A., Zhou, W., and Eglinton, T. (1994). Sulfonates: a novel class of organic sulfur compounds in marine sediments. *Geochim. Cosmochim. Acta* 58, 4681–4687. doi: 10.1016/0016-7037(94)90200-3

Vairavamurthy, M. A., Manowitz, B., Maletic, D., and Wolfe, H. (1997). Interactions of thiols with sedimentary particulate phase: studies of 3-mercaptopropionate in salt marsh sediments from Shelter Island, New York. *Organ. Geochem.* 26, 577–585. doi: 10.1016/s0146-6380(97)00019-3

van Dongen, B. E., Schouten, S., and Sinninghe Damsté, J. S. (2002). Carbon isotope variability in monosaccharides and lipids of aquatic algae and terrestrial plants. *Mar. Ecol. Prog. Ser.* 232, 83–92. doi: 10.3354/meps232083

Wakeham, S., Damste, J. S., Kohnen, M., and De Leeuw, J. W. (1995). Organic sulfur compounds formed during early diagenesis in Black Sea sediments. *Geochim. Cosmochim. Acta* 59, 521–533. doi: 10.1016/0016-7037(94)00361-o

Wanless, H. R., and Dravis, J. J. (2008). "Role of storms and prevailing energy in defining sediment body geometry, composition, and texture on caicos platform," in *Developing Models and Analogs for Isolated Carbonate Platforms: Holocene and Pleistocene Carbonates of Caicos Platform*, eds W. A. Morgan and P. M. Harris (Tulsa, OK: SEPM Society for Sedimentary Geology).

Webb, S. M. (2005). SIXpack: a graphical user interface for XAS analysis using IFEFFIT. *Phys. Scr.* 2005:1011. doi: 10.1238/Physica.Topical.115a01011

Wooller, M., Smallwood, B., Jacobson, M., and Fogel, M. (2003). Carbon and nitrogen stable isotopic variation in *Laguncularia racemosa* (L.) *(white mangrove)*. *Hydrobiologia* 499, 13–23.

Conflict of Interest Statement: The authors declare that the research was conducted in the absence of any commercial or financial relationships that could be construed as a potential conflict of interest.

Copyright © 2019 Raven, Fike, Gomes and Webb. This is an open-access article distributed under the terms of the Creative Commons Attribution License (CC BY). The use, distribution or reproduction in other forums is permitted, provided the original author(s) and the copyright owner(s) are credited and that the original publication in this journal is cited, in accordance with accepted academic practice. No use, distribution or reproduction is permitted which does not comply with these terms.